Table S1. Reaction rate expressions, rate constants (k) and ionic strength (I_s) effects for sulfate production in aerosol water.

Oxidants	Sulfate formation rate ($M\ s^{-1}$)	Notes	References
O_3	$(k_1[H_2SO_3]+k_2[HSO_3^-]+k_3[SO_3^{2-}])[O_3(aq)]$		(Hoffmann and Calvert,
	$k_1 = 2.4\times10^4\ M^{-1}\ s^{-1}$		1985)
	$k_2 = 3.7\times10^5\times e^{(-5530\times(1/T-1/298))}\ M^{-1}\ s^{-1}$		
	$k_3 = 1.5\times10^9\times e^{(-5280\times(1/T-1/298))}\ M^{-1}\ s^{-1}$		
H_2O_2	$k_4[H^+][HSO_3^-][H_2O_2(aq)]/(1+K[H^+])$		(Mcardle and Hoffmann,
	$k_4 = 7.45\times10^7\times e^{(-4430\times(1/T-1/298))}\ M^{-1}\ s^{-1}$		1983)
	$K = 13\ M^{-1}$		
	$EF^{\,a} = 10(3.055\log(I_s)-1.919)$	$I_{s,\ max} = 14.5\ M$	(Liu et al., 2020)
NO_2	$k_5[S(IV)][NO_2(aq)]$		(Clifton et al., 1988; Lee and
	$k_{5low} = 2\times10^6\ M^{-1}\ s^{-1}$		Schwartz, 1982)
	$k_{5high} = (1.24-2.95)\times10^7\ M^{-1}\ s^{-1}$		
O_2	$k_6[H^+]^{-0.74}[S(IV)][Mn(II)][Fe(III)]\ (pH \leq 4.2)$		(Ibusuki and Takeuchi, 1987)
	$k_6 = 3.72\times10^7\times e^{(-8431.6\times(1/T-1/297))}\ M^{-2}\ s^{-1}$		
	$k_7[H^+]^{0.67}[S(IV)][Mn(II)][Fe(III)]\ (pH > 4.2)$		
	$k_7 = 2.51\times10^{13}\times e^{(-8431.6\times(1/T-1/297))}\ M^{-2}\ s^{-1}$		
	$\log_{10}\left(\dfrac{k}{k^{I_s=0}}\right) = \dfrac{b_1\sqrt{I_s}}{1+\sqrt{I_s}}$	$I_{s,\ max} = 2.3\ M$	(Liu et al., 2020)
		$b_1 = -3.02$	

[a] Enhancement factor accounts for the overall effects of ionic strength on the reaction rate constant k, Henry's law constants of H_2O_2 and SO_2, and the first-order dissociation constant of H_2SO_3. The expression was got by personal communication.

Table S2. The mean and ranges of surface $PM_{2.5}$ pH at sampling site in each scenario during clean, light pollution, moderate pollution, heavy pollution periods as well as the entire period.

Scenarios	Clean		Light		Moderate		Heavy		Entire period	
	range	mean	range	mean	range	mean	range	mean	range	mean
ORIG	1.10-7.12	3.20	1.06-6.77	2.12	0.98-2.63	1.58	0.93-2.54	1.41	0.93-7.12	2.33
CTL1	1.71-7.51	4.68	1.37-7.34	2.68	1.27-3.12	2.18	1.21-3.01	1.91	1.21-7.51	3.22
CTL2	2.35-7.54	5.04	2.24-7.35	3.60	2.25-3.80	3.29	2.09-3.81	3.13	2.09-7.54	3.93
CTL3	2.35-7.54	4.90	2.25-7.35	3.53	2.38-3.75	3.26	1.97-3.76	3.06	1.97-7.54	3.85
CTL3meta	2.36-7.67	4.77	2.25-7.33	3.41	2.39-3.60	3.19	2.10-3.64	3.02	2.10-7.67	3.75
CTL3het_NoIs	1.84-7.63	5.23	1.21-7.36	3.48	1.05-3.46	2.56	0.64-3.21	1.73	0.64-7.63	3.07
CTL3het_Is	2.28-7.70	4.89	2.19-7.35	3.48	2.42-3.70	3.18	1.92-3.71	2.96	1.92-7.70	3.78

Table S3. The concentrations (in unit of $\mu mol\ m^{-3}$) of major $PM_{2.5}$ components for each bin (01-06) averaged over the pH-decreasing regions in CTL3meta scenario.

Size bin	Ca^{2+}	Na^+	SO_4^{2-}	NH_4^+	NO_3^-	Cl^-
bin 01	0.0001	0.0003	0.0006	0.0009	0.0001	0.0001
bin 02	0.0001	0.0003	0.0012	0.0020	0.0001	0
bin 03	0.0005	0.0006	0.0025	0.0036	0.0001	0.0001
bin 04	0.0032	0.0017	0.0025	0.0013	0.0006	0.0012
bin 05	0.0135	0.0053	0.0009	0	0.0035	0.0053
bin 06	0.0426	0.0164	0.0006	0	0.0061	0.0164
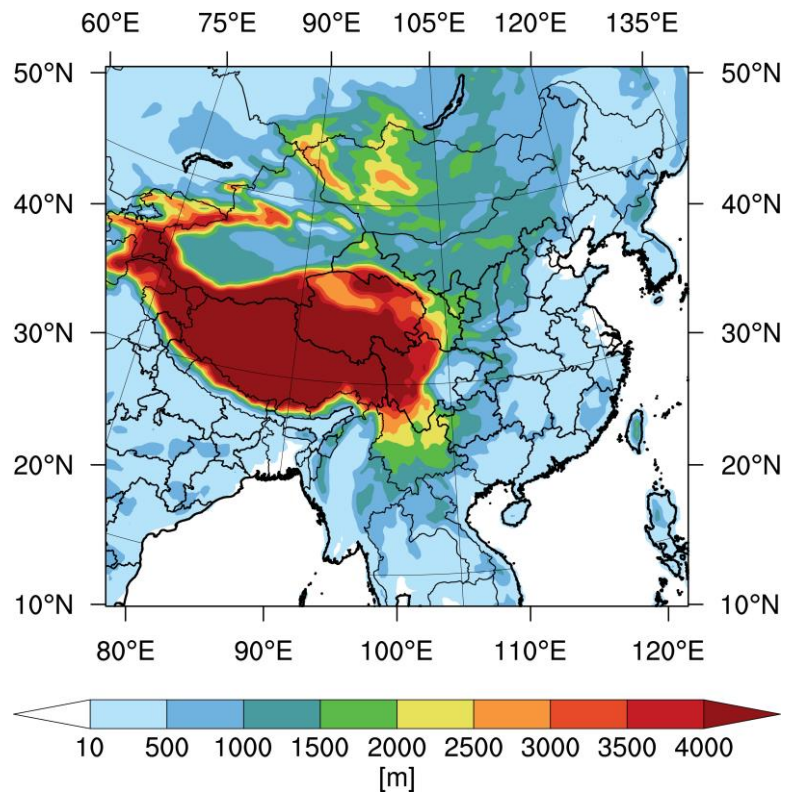
Figure S1. Simulation domain. The color shading represents the topography height (m).
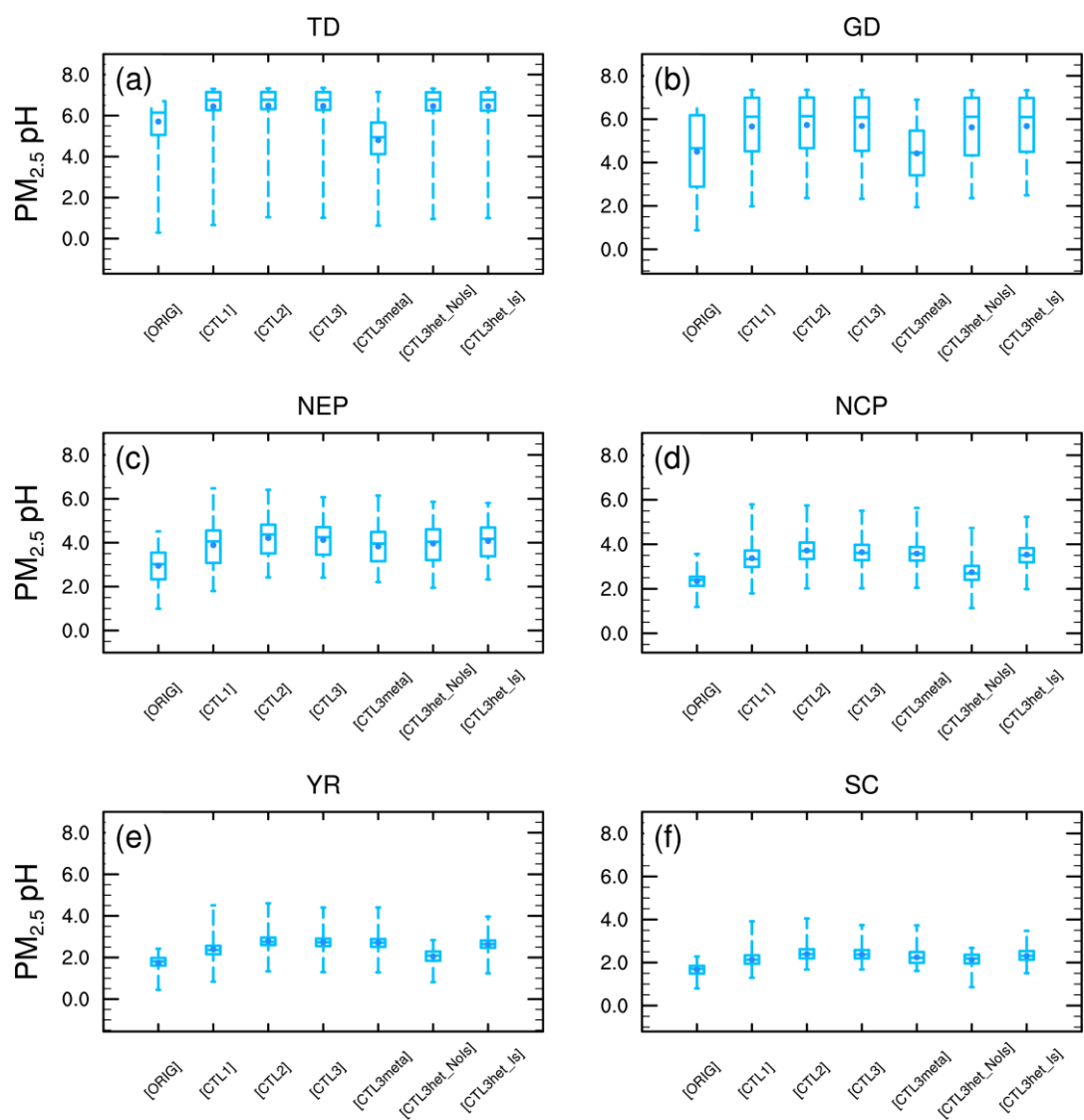
Figure S2. Boxplots of surface PM$_{2.5}$ pH simulated by each scenarios over (a) TD, (b) GD, (c) NEP, (d) NCP, (e) YR, (f) SC. The boxes represent, from top to bottom, the 75th, 50th, and 25th percentiles of statistical data. The whiskers represent, from top to bottom, the minimum and the maximum, and the solid circles represent the mean values.
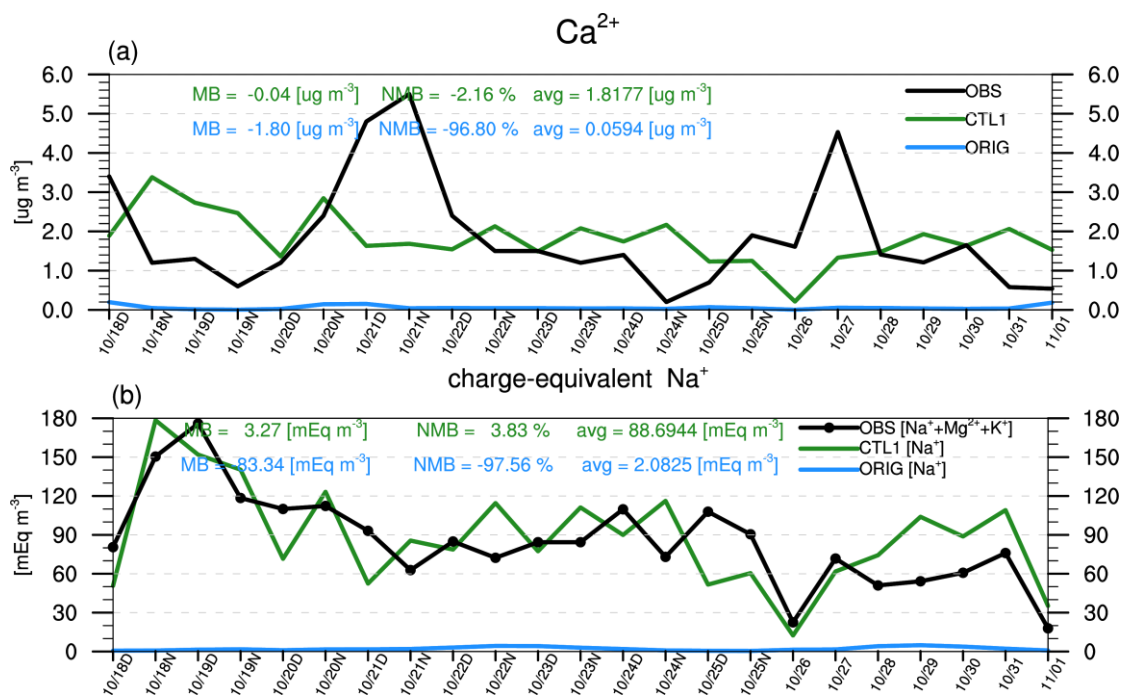
Figure S3. Comparison of simulated (a) Ca^{2+} concentration (μg m^{-3}) and (b) Na$^+$ concentration (mEq m^{-3}) with observations

(OBS; black line) for ORIG (blue line) and CTL1 (green line) scenarios at Beijing site during the study period of 15 October

2014 - 02 November 2014, with the mean bias (MB), normalized mean bias (NMB) and average value (avg) given insert. MB

and NMB are defined as $MB = \frac{1}{N}\sum_1^N C_m - C_o$ and $NMB = \frac{\sum_1^N C_m - C_o}{\sum_1^N C_o}$, where C_m is the modeled value, C_o is the observed value,

and N is the number of paired model and observation data. Mg^{2+} and K$^+$ are treated as charge-equivalent Na$^+$. "D" and "N" on

the x-axis indicate day and night sampling periods, respectively. Dates without "D" and "N" indicate 24-h samples.
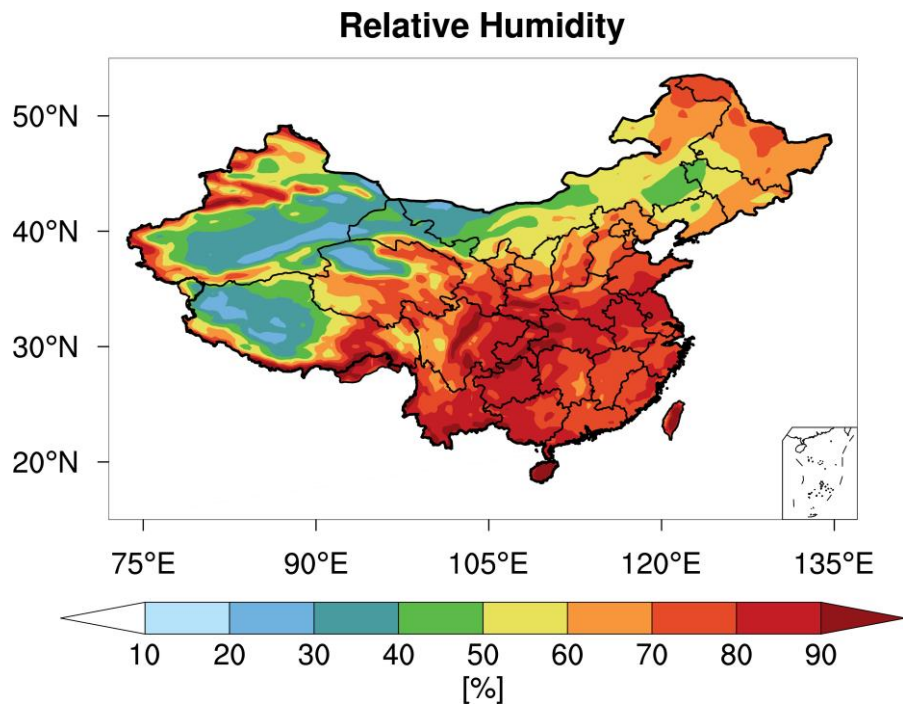
Figure S4. Spatial distribution of mean surface relative humidity [%] from WRF-Chem during the study period of 15 October
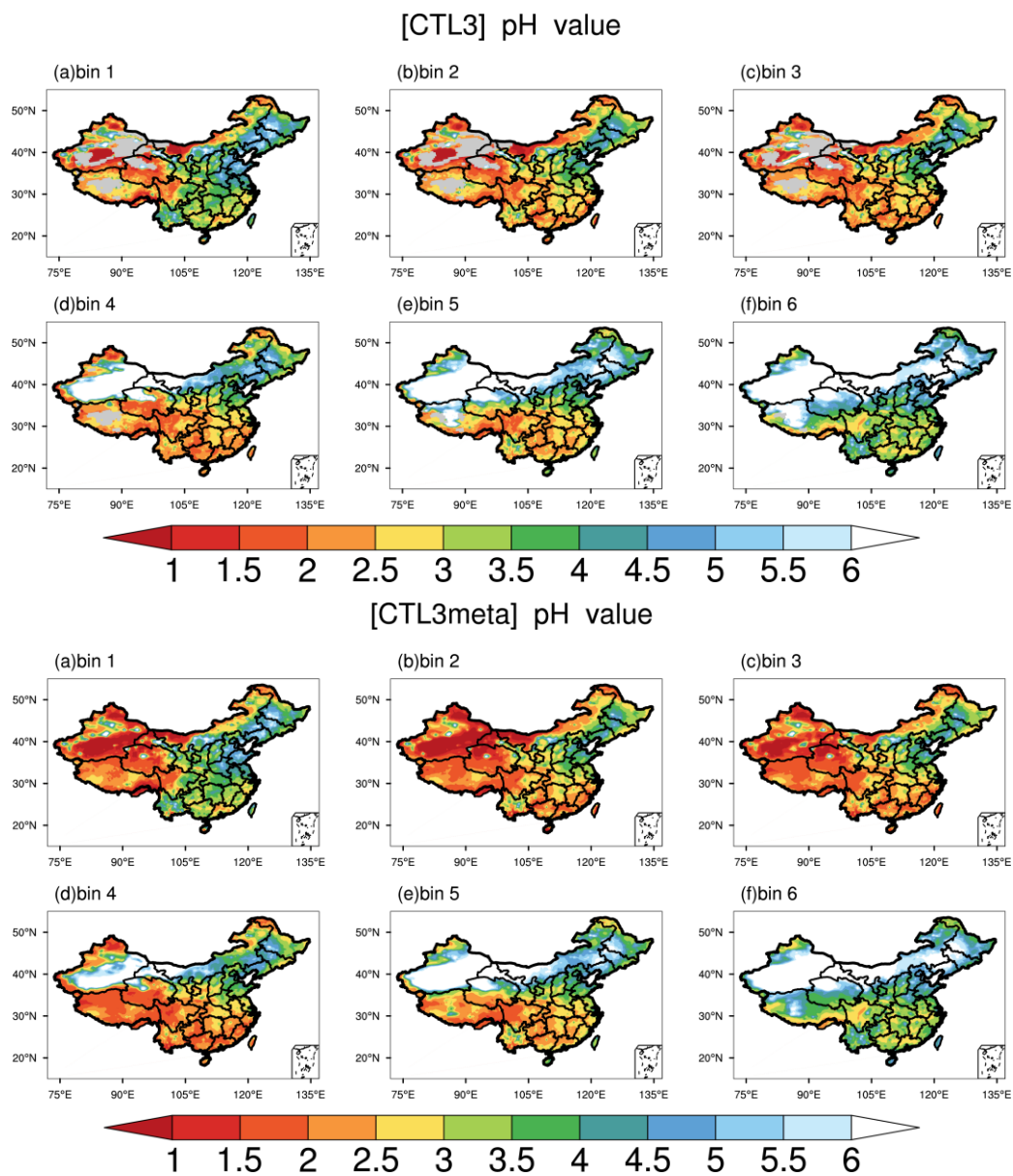
2014 - 02 November 2014.

Figure S5. Spatial distributions of mean surface aerosol pH during the study period of 15 October 2014 - 02 November 2014 predicted by (top panel) CTL3 scenario and (bottom panel) CTL3meta scenario for six size bins. (a) Bin 1 for 0.039-0.078 μm diameter, (b) Bin 2 for 0.078-0.156 μm diameter, (c) Bin 3 for 0.156-0.312 μm diameter, (d) Bin 4 for 0.312-0.625 μm diameter, (e) Bin 5 for 0.625-1.25 μm diameter, (f) Bin 6 for 1.25-2.5 μm diameter.
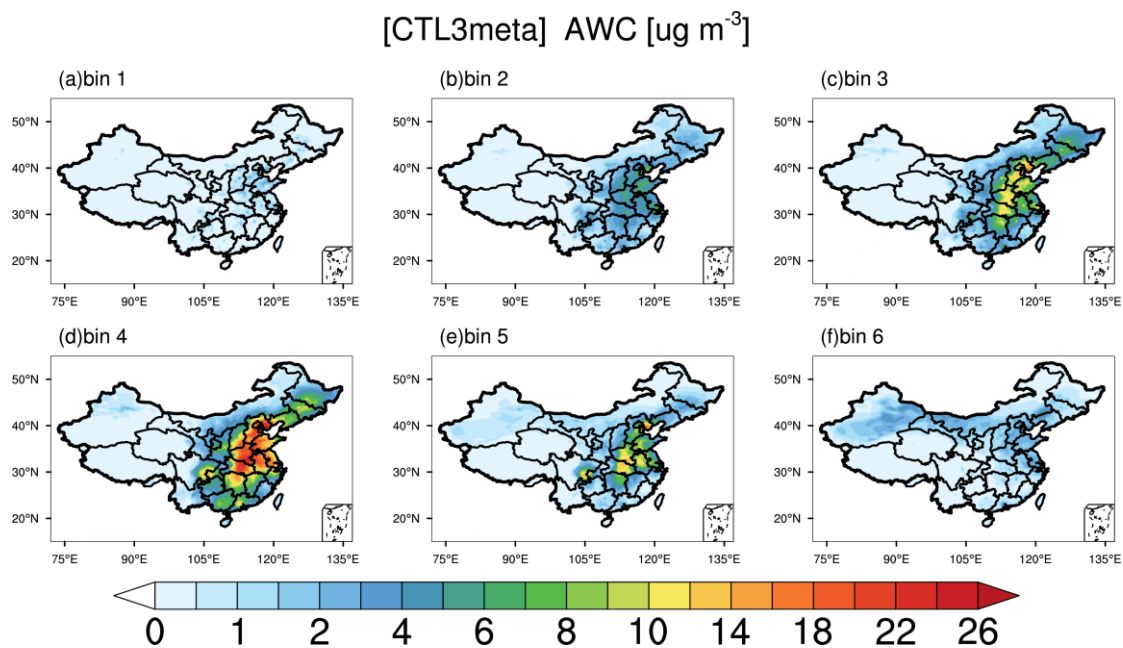
Figure S6. Spatial distributions of AWC (μg m⁻³) during the study period of 15 October 2014 - 02 November 2014 predicted by CTL3meta scenario for six size bins. (a) Bin 1 for 0.039-0.078 μm diameter, (b) Bin 2 for 0.078-0.156 μm diameter, (c) Bin 3 for 0.156-0.312 μm diameter, (d) Bin 4 for 0.312-0.625 μm diameter, (e) Bin 5 for 0.625-1.25 μm diameter, (f) Bin 6 for 1.25-2.5 μm diameter.
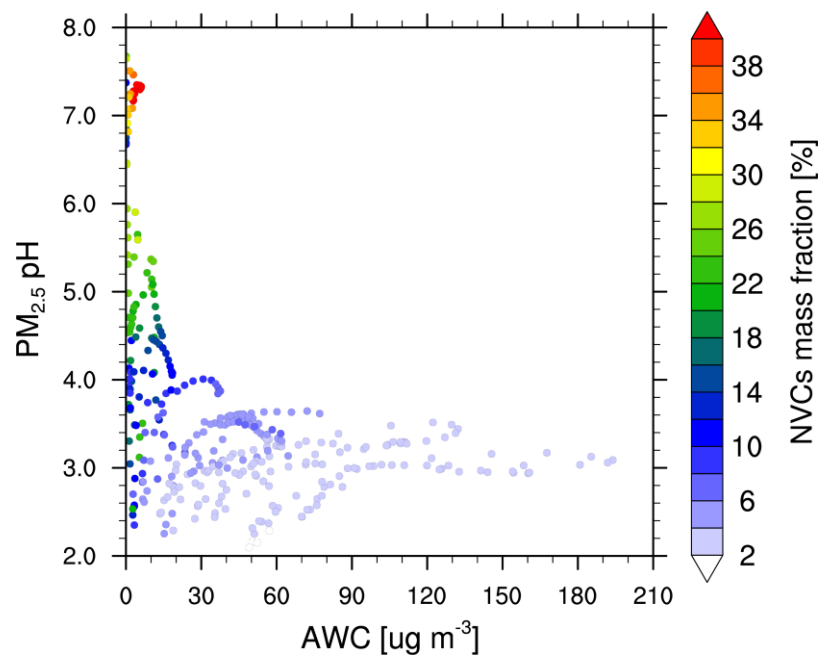
Figure S7. Scatter plots of modeled surface $PM_{2.5}$ pH vs. AWC ($\mu g\ m^{-3}$) colored with NVCs mass fraction (%) from CTL3meta

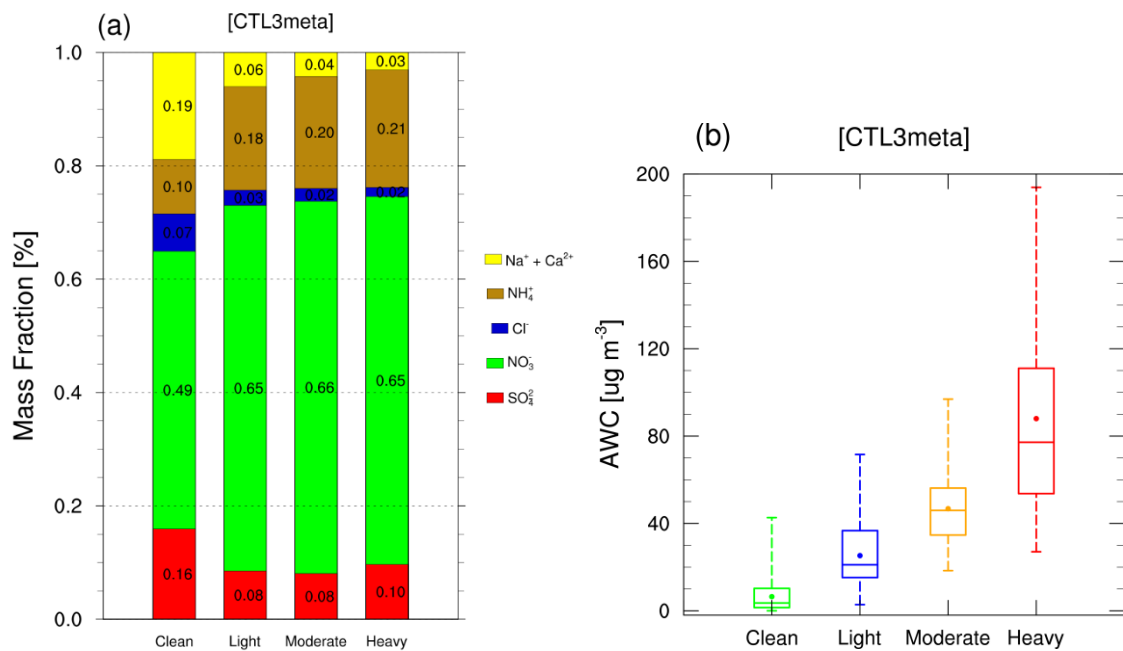scenario for data at Beijing site during the study period of 15 October 2014 - 02 November 2014.

Figure S8. Modeled (a) mass fractions [%] of PM$_{2.5}$ ionic species and (b) AWC (μg m^{-3}) from CTL3meta scenario in each haze stage.
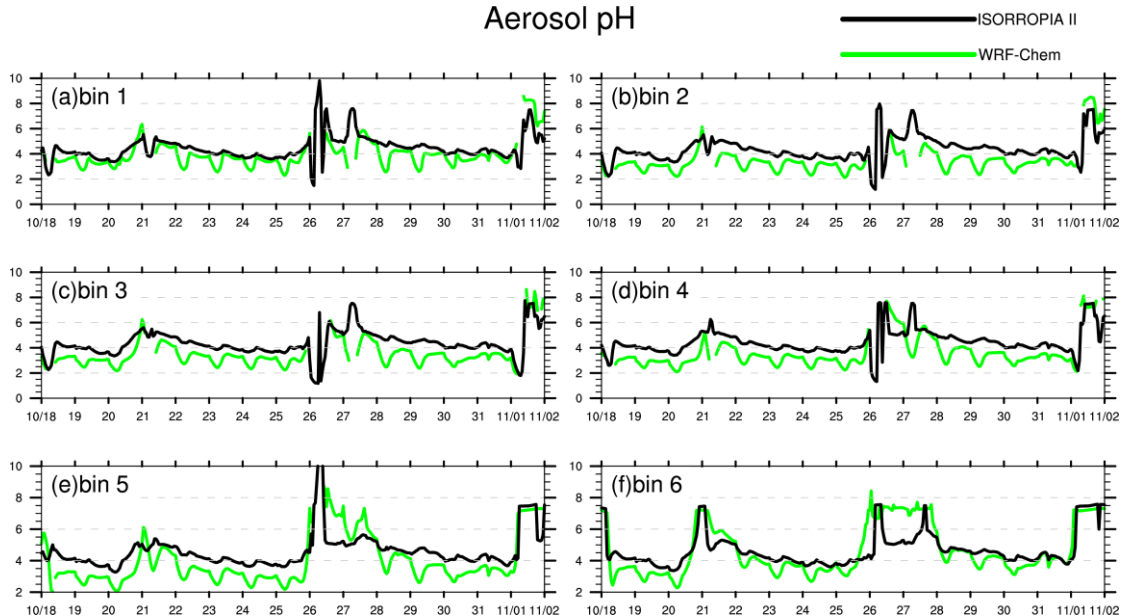
Figure S9. Time series of aerosol pH (bin01-bin06) calculated by WRF-Chem (CTL3meta, green line) and ISORROPIA II (black line) at the surface in Beijing. ISORROPIA II ("forward" mode, assuming metastable) was run with WRF-Chem simulated hourly chemical concentrations along with T and RH.
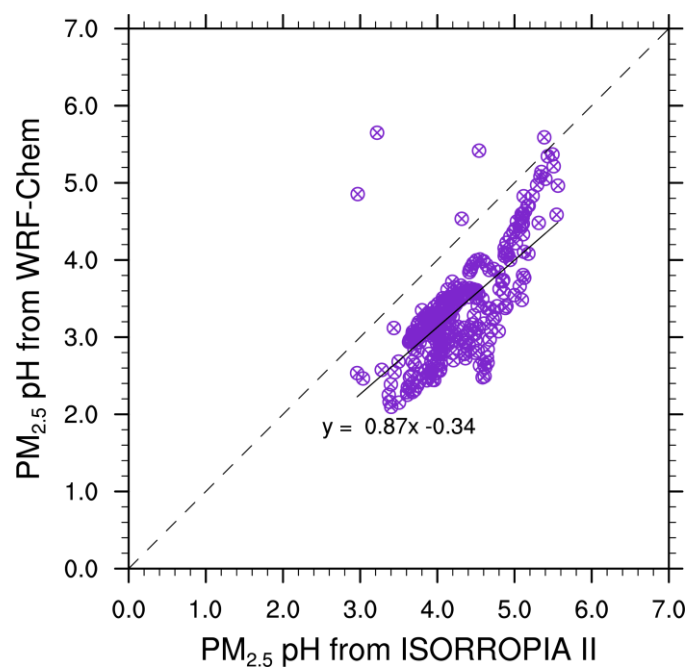
Figure S10. PM$_{2.5}$ pH predicted by WRF-Chem against the corresponding pH predicted using ISORROPIA II for the data

presented in Fig. S9. PM$_{2.5}$ pH is calculated using LWC-weighted average from bin 01~bin 06. The dashed line denotes the 1:
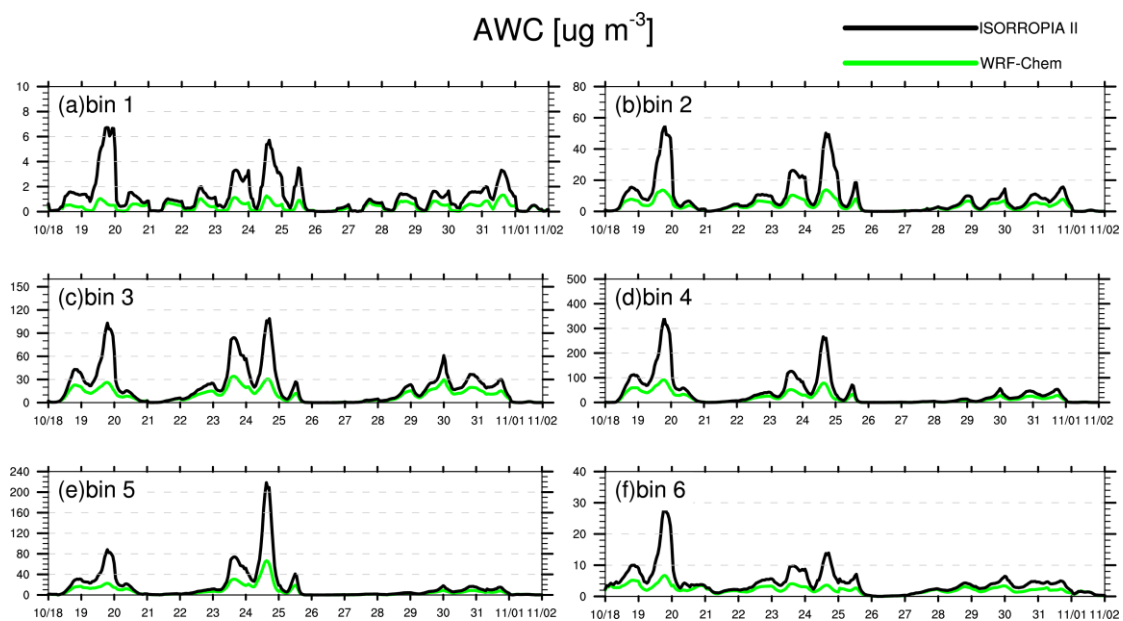
1 line. Linear regression fit is shown.

Figure S11. Same as Fig. S9, but for AWC (μg m⁻³).

References

Clifton, C. L., Altstein, N., and Huie, R. E.: Rate constant for the reaction of nitrogen dioxide with sulfur(IV) over the pH range 5.3-13, Environ. Sci. Technol., 22, 586-589, https://doi.org/10.1021/es00170a018, 1988.

Hoffmann, M. R., and Calvert, J. G.: Chemical Transformation Modules for Eulerian Acid Deposition Models. Volume 2. The Aqueous-Phase Chemistry., Atmospheric Sciences Research Laboratory, Office of Research and Development, US Environmental Protection Agency, 1985.

Ibusuki, T., and Takeuchi, K.: Sulfur-Dioxide Oxidation by Oxygen Catalyzed by Mixtures of Manganese(II) and Iron(III) in Aqueous-Solutions at Environmental Reaction Conditions, Atmos. Environ., 21, 1555-1560, https://doi.org/10.1016/0004-6981(87)90317-9, 1987.

Lee, Y. N., and Schwartz, S. E.: Kinetics of oxidation of aqueous sulfur(IV) by nitrogen dioxide, Conference: 4. international conference on precipitation scavenging, dry deposition and resuspension, Santa Monica, CA, USA, 29 Nov 1982, ; Brookhaven National Lab., Upton, NY (USA), Medium: X; Size: Pages: 15 pp., 1982.

Liu, T., Clegg, S. L., and Abbatt, J. P. D.: Fast oxidation of sulfur dioxide by hydrogen peroxide in deliquesced aerosol particles, Proc. Natl. Acad. Sci. U. S. A., 117, 1354-1359, https://doi.org/10.1073/pnas.1916401117, 2020.

Mcardle, J. V., and Hoffmann, M. R.: Kinetics and Mechanism of the Oxidation of Aquated Sulfur-Dioxide by Hydrogen-Peroxide at Low pH, J. Phys. Chem., 87, 5425-5429, https://doi.org/10.1021/j150644a024, 1983.